Volume 12
Number 11
21 March 2020
Pages 6213-6584

Nanoscale

rsc.li/nanoscale

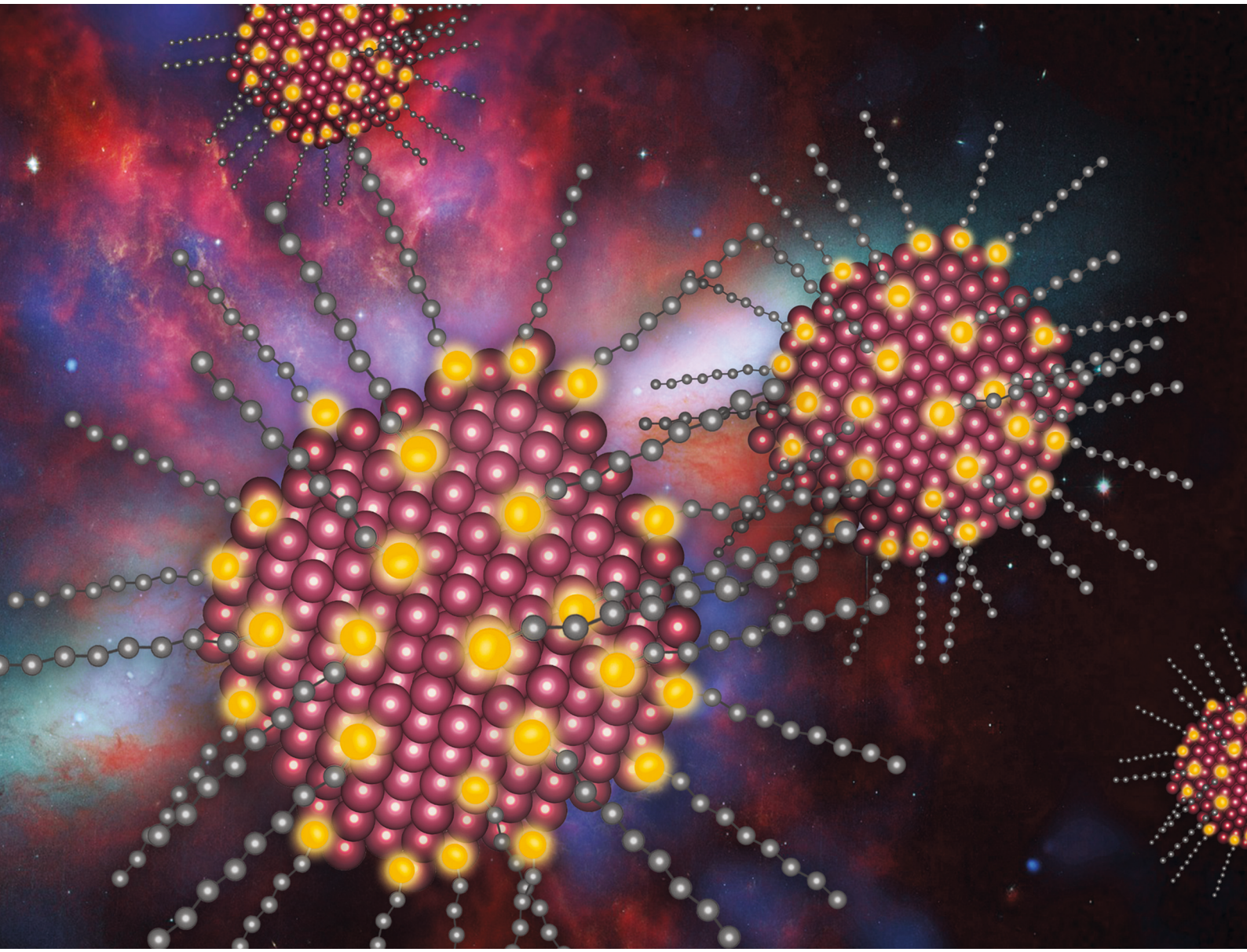

ISSN 2040-3372

ROYAL SOCIETY OF CHEMISTRY

PAPER
Jonathan G. C. Veinot *et al.*
Dehydrocoupling – an alternative approach to functionalizing germanium nanoparticle surfaces

NCNST

Nanoscale

PAPER

View Article Online
View Journal | View Issue

Cite this: *Nanoscale*, 2020, **12**, 6271

Dehydrocoupling – an alternative approach to functionalizing germanium nanoparticle surfaces†

Md Asjad Hossain, [a] Morteza Javadi, [a] Haoyang Yu, [a] Alyxandra N. Thiessen, [a] Nduka Ikpo, [a] Anton O. Oliynyk [a,b] and Jonathan G. C. Veinot *[a]

Received 24th December 2019,
Accepted 4th February 2020

DOI: 10.1039/c9nr10837h

rsc.li/nanoscale

Surface functionalization is an essential aspect of nanoparticle design and preparation; it can impart stability, processability, functionality, as well as tailor optoelectronic properties that facilitate future applications. Herein we report a new approach toward modifying germanium nanoparticle (GeNP) surfaces and for the first time tether alkyl chains to the NP surfaces through Si–Ge bonds. This was achieved *via* heteronuclear dehydrocoupling reactions involving alkylsilanes and Ge–H moieties on the NP surfaces. The resulting solution processable RR′$_2$Si–GeNPs (R = octadecyl or PDMS; R′ = H or CH_3) were characterized using FTIR, Raman, ^{1}H-NMR, XRD, TEM, HAADF, and EELS and were found to retain the crystallinity of the parent GeNP platform.

Introduction

Germanium nanoparticles (GeNPs) are promising materials that may find use as active systems in far reaching applications, such as solar cells, batteries, field-effect transistors, data storage devices, metamaterials, and photodetectors.[1–7] Their vast potential arises partly because bulk germanium has a comparatively small band gap (0.67 *vs.* 1.1 eV in silicon) and large exciton Bohr radius (~24 *vs.* 4.9 nm in silicon) which lead to predictions that the influence of quantum confinement will be observed in *large* particles.[1] These *larger* nanoparticles are particularly attractive because they should maintain size and shape tunable properties while being *more* resistant to deleterious surface reactions (*e.g.*, oxidation). Still, GeNP surfaces remain sensitive to air and moisture.[8,9]

Drawing on the well-established hydrosilylation approaches used to tailor silicon surface chemistry and the perceived similarities of silicon and germanium reactivity, we and others explored hydrogermylation as one approach for modifying the surfaces of bulk and nanoscale Ge.[8,10–16] Despite these early advances, challenges remain, and investigating the surface chemistry of germanium nanomaterials, particularly GeNPs, is of paramount importance if their attractive properties are to be exploited.

Dehydrocoupling (DHC) reactions involve the formal liberation of H_2 upon reaction of two M–H (*e.g.*, M = Si and/or Ge) species, resulting in the formation of an M–M bond; this general reaction has proven effective in Group 14 element molecular chemistry.[17,18] Applications of the DHC reaction have also been extended to the modification of bulk and nanoscale Group 14 semiconductor surfaces. Li *et al.*[19] derivatized H-terminated silicon wafers and porous-Si surfaces *via* zirconocene and titanocene catalyzed DHC; these reactions introduced arylsilanes or alkylsilanes to the surface. Drawing inspiration from these studies, we extended DHC to reactions of alkylsilanes with H-terminated SiNPs using Wilkinson's catalyst ($(PPh_3)_3RhCl$). While surface modification was achieved, the utility of this approach was limited because the material optical properties were compromised.[20] An important step forward was realized when Kim *et al.*[21] demonstrated DHC could be thermally-initiated on porous-Si surfaces in the absence of a metal-based catalysts – this advance made it possible to functionalize *via* DHC while maintaining the substrate photoluminescence. However, it is important to note that the reaction products possessed substantial surface oxide.

Homonuclear DHC of arylgermanes has been used in the preparation of oligo- and poly-germanes.[22] To date it has not been applied as a strategy for modifying bulk or nanoscale Ge surfaces. Reaching beyond the mere curiosity of whether DHC will provide a viable approach for tailoring GeNPs, establishing heteronuclear dehydrocoupling protocols involving GeNP surfaces and alkylsilanes (*i.e.*, $RSiH_3$ or RR′$_2$SiH) may provide a solution-based method for introducing crystal strain-induced band gap engineering in "core–shell" nanoparticles of Group 14 elements that have, of late, been the subject of computational and gas-phase synthesis investigations.[23–27] In this regard, we demonstrate the successful modification of H-terminated GeNPs *via* the DHC with a series of alkylsilanes.

[a]*Department of Chemistry, University of Alberta, T6G 2G2 Canada. E-mail: jveinot@ualberta.ca*
[b]*Manhattan College, Riverdale, New York, 10471, USA*

†Electronic supplementary information (ESI) available. See DOI: 10.1039/c9nr10837h

Experimental

Reagents and materials

Germanium dioxide powder (GeO_2, 99.9%) and octadecyldimethylsilane were purchased from Gelest. Aqueous hypophosphorous acid (50 wt%), sodium hydroxide pellets, toluene (99.9%, HPLC grade), 1-octadecene (90%), octadecylsilane (97%), H-terminated poly(dimethylsiloxane) (H-PDMS, average $M_n \sim 580$), chloroform-D (99.8%) with 0.03% tetramethyl silane (TMS), dodecane (99%), and acetonitrile (99.9%, HPLC grade) were purchased from Sigma-Aldrich. Toluene and acetonitrile were purified using a Pure-Solv system and collected immediately prior to use. Hydrochloric acid (36.5–38.0%) and ammonium hydroxide (28–30%) were purchased from Caledon Labs. Electronics grade hydrofluoric acid (HF, 49% aqueous solution) was purchased from J. T. Baker. Ultrapure H_2O (18.2 MΩ cm^{-1}) was obtained from a Barnstead Nanopure Diamond purification system and was used in all reactions. Molecular sieves (4 Å) were purchased from Sigma-Aldrich and activated in a vacuum oven prior to use. Unless otherwise indicated, reagents were used as received.

Preparation of GeNPs embedded in germanium oxide

GeNPs embedded in a germanium oxide matrix (GeNP/GeO_x) were prepared using a procedure developed in our laboratory.[15] Briefly, $Ge(OH)_2$ was prepared by dissolving 2.0 g of GeO_2 in 14 mL freshly prepared aqueous NaOH (~17 M) in a 250 mL round bottom flask. Subsequently, aqueous HCl (6 M, 48 mL) was added dropwise to the solution to achieve a pH ~ 1. Next, aqueous hypophosphorus acid (50 wt% H_3PO_2; 15 mL) was added and the mixture was refluxed for 5.5 h under static argon. Concentrated NH_4OH (20 mL) was added to the boiling reaction mixture to yield a brown precipitate that was isolated by vacuum filtration and washed three times with 10 mL aliquots of ultrapure water. After drying in a vacuum oven at *ca.* 70 °C for 15 h, 1.6 g of '$Ge(OH)_2$' was obtained. This brown powder (1.0 g) was placed in a quartz boat and heated in a Lindberg Blue tube furnace under flowing argon (15 mL min^{-1}). The furnace temperature was ramped to 400 °C (18 °C min^{-1}) where it remained for 1 h. After cooling to room temperature, a dark brown solid consisting of GeNPs embedded in germanium oxide (GeNP/GeO_x) was obtained and ground to a fine powder using an agate mortar and pestle. The resulting material (*ca.* 1.0 g) was characterized using X-ray powder diffraction and stored in ambient atmosphere until needed.

Isolation of hydride-terminated GeNPs

H-terminated GeNPs (H-GeNPs) were liberated from the GeNP/GeO_x *via* ethanolic hydrofluoric acid (HF) etching using a literature procedure.[15] (Caution! HF must be handled with extreme care and in accordance with local regulations.) Briefly, GeNP/GeO_x (0.2 g) was placed in a polyethylene terephthalate beaker, followed by absolute ethanol (2.0 mL). This mixture was exposed to an ultrasonic bath for approximately 2 min, after which, ultrapure water was added (2.0 mL), and the heterogeneous brown mixture was stirred using a magnetic stir bar/stir plate for 10 min. Subsequently, aqueous HF (49% HF; 2.0 mL) was added. After stirring for 15 min, the liberated H-GeNPs were collected upon extraction into toluene (3 × 10 mL) to yield a dark brown cloudy dispersion and were isolated as a brown pellet upon centrifugation at 3000 rpm. The H-GeNPs were re-dispersed in toluene containing activated molecular sieves and stirred. The molecular sieves were removed, and the mixture was centrifuged at 3000 rpm to recover the H-GeNPs (*ca.* 20% mass yield). This process was repeated and the obtained H-GeNPs were derivatized immediately using the DHC or hydrogermylation conditions noted below.

Dehydrocoupling on H-GeNPs surfaces

The H-GeNPs obtained from etching 0.2 g of GeNP/GeO_x were dispersed in dodecane (5 mL, dried over activated molecular sieves), transferred to a Schlenk flask equipped with a Teflon coated stir bar, and attached to an argon charged double manifold. Subsequently, 3.5 mmol of the alkylsilane of choice and an additional 15 mL dry dodecane were added. The cloudy reaction mixture was subjected to three freeze–pump–thaw cycles and then heated in an oil bath at 180 °C for 96 h with stirring. After cooling, the cloudy crude product mixture was transferred to polytetrafluoroethylene (PTFE) centrifuge tubes, and toluene (3 mL) was used to collect all the samples from the Schlenk flask. Subsequently, acetonitrile (30 mL) was added as an antisolvent. The resulting brown suspension was centrifuged at 12 000 rpm for 30 min to yield a brown precipitate and a colorless supernatant. The supernatant was discarded, and the solid was re-dispersed in 5 mL of toluene with sonication to yield a cloudy suspension. Subsequently, acetonitrile (45 mL) was added, and the mixture was centrifuged at 12 000 rpm for 30 min to yield a brown solid. This solvent/antisolvent suspension/precipitation procedure was repeated once. Finally, the precipitate (*i.e.*, alkylsilane functionalized GeNPs) was dispersed in 5 mL of dry toluene, and stored in a vial at ambient conditions for further use and characterization.

Hydrogermylation of H-GeNPs surfaces

An established literature procedure was employed to modify GeNP surfaces *via* thermally-induced hydrogermylation.[15] These materials provide a baseline comparison for functionalized GeNPs obtained from DHC reactions. Briefly, H-GeNPs liberated from the identical GeNP/GeO_x were mixed with neat 1-octadecene (10 mL) and heated in an oil bath at 180 °C for 96 h with stirring. The resulting octadecyl-terminated GeNPs were purified and stored using the identical procedure outlined for the DHC products.

Materials characterization and instrumentation

Fourier Transform Infrared spectroscopy (FTIR) was performed using a Nicolet Magna 750 IR spectrophotometer. Samples were prepared by drop casting from a toluene suspension onto a silicon wafer.

Proton nuclear magnetic resonance spectroscopy (^{1}H NMR) was performed using a Varian Unity Inova Console 500 MHz

NMR spectrometer. Signals were calibrated in MestReNova (version 9.0.1-13254) using TMS (0 ppm) standard and intensity ratios were obtained. Samples were prepared such that they contained a few milligrams of GeNPs in 0.03% TMS in 0.6 mL $CDCl_3$.

A Renishaw inVia Raman microscope equipped with a 633 nm diode laser and using a 50% laser power was used to obtain Raman spectra. Samples were prepared by drop casting of a toluene NP suspension on to a gold coated glass slide.

X-ray diffraction was performed using Rigaku Ultima IV equipped with a Cu-Kα radiation source (λ = 1.54 Å) using a thin film stage. The $Ge(OH)_2$ and $GeNP/GeO_x$ samples were prepared by placing the powder sample on a 10 × 10 mm^2 Si (100) wafer. Functionalized GeNPs samples were prepared by drop casting on to a 10 × 10 mm^2 Si (100) wafer. XRD data were refined and analyzed using the TOPAS Academic software package.

X-ray photoelectron spectra were obtained in energy spectrum mode at 210 W using Kratos Axis Ultra X-ray photoelectron spectrometer. The X-ray source was Al Kα (1486.6 eV). Samples were prepared on a copper foil (5 × 5 mm^2) substrate. CasaXPS (version 2.3.13) was used to calibrate binding energies using the C 1s peak as a reference (284.8 eV). A Shirley-type background was applied. The C 1s region was fit/deconvoluted to determine the amount of oxide arising from adventitious carbon. The Ge 3d region of the XPS was fit to Ge $3d_{3/2}$ and Ge $3d_{5/2}$ partner lines with spin–orbit splitting fixed at 0.58 eV and intensity ratio at 0.67. The Si 2p region was fit to Si $2p_{1/2}$ and $2p_{3/2}$ partner lines with spin–orbit splitting at 0.6 and intensity ratio at 0.5.

Bright-field transmission electron microscopy (TEM), high-resolution TEM (HRTEM), and energy dispersive X-ray (EDX) were performed in JEOL JEM-ARM200CF equipped with cold field emission gun (cFEG) having an accelerating voltage of 200 kV. High angular annular dark field (HAADF) imaging and electron energy loss spectroscopy (EELS) were acquired in scanning mode with a nominal electron probe size of 0.5 nm using JEOL 2200 FS TEM/STEM. TEM samples were prepared by drop-coating 1–2 drops of dilute toluene GeNP suspension containing on to a holey carbon coated copper grid (150 mesh, Electron Microscopy Science). Bright-field TEM and HRTEM images were processed using ImageJ software (version 1.51j8) and at least 300 particles were measured to obtain size distributions.

Dynamic light scattering (DLS) data was obtained using a Malvern Zetasizer Nano S series equipped with a 633 nm laser. All the toluene suspension containing functionalized GeNP samples were equilibrated to 25 °C prior to data acquisition and scanned three times.

Results and discussion

Oxide-embedded germanium nanoparticles ($GeNP/GeO_x$) were prepared using procedures developed in our laboratory that exploit the thermal disproportionation of '$Ge(OH)_2$'.[15]

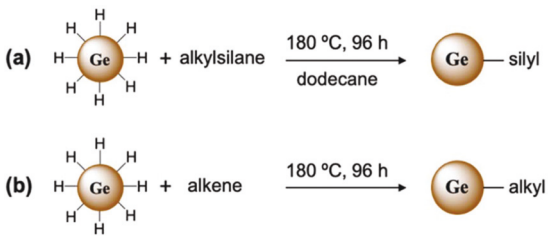

Scheme 1 Protocols for functionalizing H-GeNPs *via* (a) dehydrocoupling, and (b) hydrogermylation.

Subsequent removal of the protective oxide matrix provided H-terminated GeNPs (H-GeNPs) that served as substrates for DHC and the hydrogermylation reactions presented in Scheme 1.

Briefly, H-GeNPs that were extracted from HF were washed with toluene and dried over molecular sieves. They were subsequently combined with dodecane and the alkylsilane of choice in a Schlenk flask and the degassed mixture was heated at 180 °C for 96 h under an Ar atmosphere with stirring. For hydrogermylation reactions, the dried H-GeNPs were combined with 1-octadecene and exposed to the same conditions noted for the DHC reactions.

Qualitative evaluation of the effectiveness of surface functionalization reactions with octadecylsilane were investigated at different reaction times and temperatures. The extent of reaction progress was qualitatively determined based upon visual inspection of intensity of the amber color of the PTFE (0.45 μm) filtered reaction mixture (Fig. S1 and S2†). Product mixtures obtained from higher reaction temperatures and longer times (at T = 180 °C, t = 96 h) appear more intensely coloured, consistent with more complete functionalization. In all cases, the FTIR features of octadecylsilyl-GeNPs at *ca.* 2960–2850 cm^{-1}, *ca.* 1464 cm^{-1}, and *ca.* 2157 cm^{-1} are associated with C–H_x stretching, C–H_x bending, and Si–H stretching, respectively (Fig. S1 and S2†). The O–H (*ca.* 3200–3600 cm^{-1}) functionalities are believed to result from partial oxidation that occurs during purification. In Fig. S1,† we note octadecylsilyl-GeNPs exhibit a weak feature associated with Ge–H (*ca.* 2015 cm^{-1}) when prepared at 80 °C; this feature is not present in samples prepared at higher T (*i.e.*, 130 and 180 °C). In addition, the intensity of the broad O–H stretching feature at *ca.* 3200–3600 cm^{-1} diminishes when the reaction was performed at higher temperature. Comparing the products obtained at different reaction times (*i.e.*, 24, 48, and 96 h) we observe the disappearance of features associated with Ge–H and O–H stretching at longer reaction times suggesting more complete functionalization (Fig. S2†).

After identifying appropriate DHC conditions, we chose octadecylsilane, dimethyloctadecylsilane, and H-PDMS as silane ligands to present the versatility of the DHC reaction. Hydrogermylation also was employed using 1-octadecene to provide a comparative functionalized GeNP sample. The FTIR of functionalized GeNPs and the corresponding ligands are shown in Fig. 1a and b, respectively. In all cases, the features

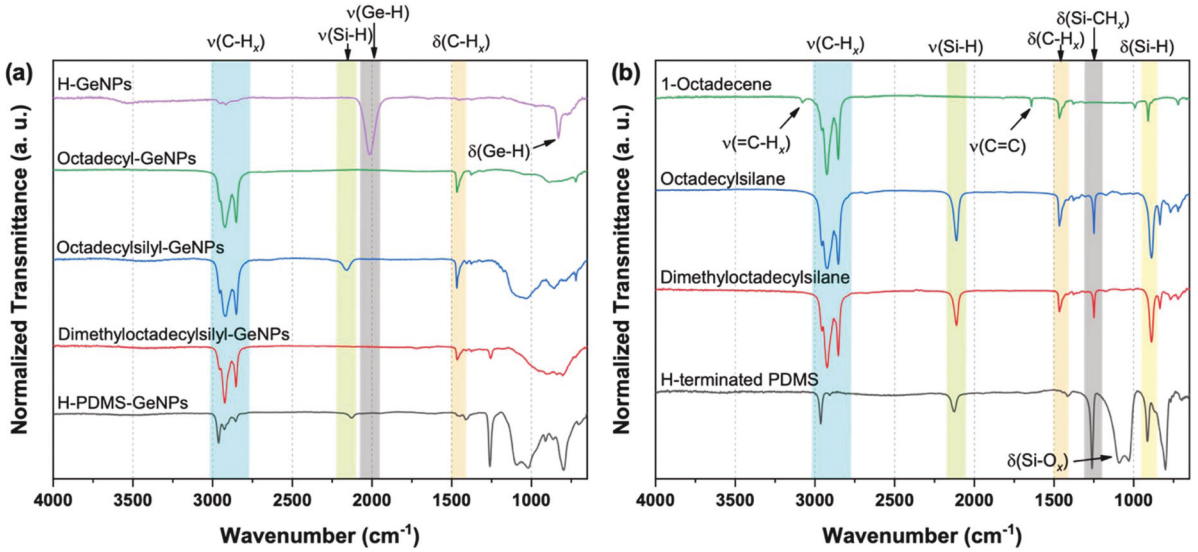

Fig. 1 FTIR spectra of (a) H-GeNPs, octadecyl-GeNPs, octadecylsilyl-GeNPs, dimethyloctadecylsilyl-GeNPs, and H-PDMS-GeNPs and (b) 1-octadecene, octadecylsilane, dimethyloctadecylsilane, and H-PDMS.

associated with target surface functionalities are observed. The spectrum obtained for H-GeNPs shows two distinctive absorptions at *ca.* 2009 and *ca.* 843 cm^{-1} arising from Ge–H stretching and bending, respectively. Following DHC and hydrogermylation reactions, the Ge–H features are no longer evident and are replaced by intense absorptions at *ca.* 2960–2850 cm^{-1} and *ca.* 1469 cm^{-1} attributed to C–H_x stretching and bending modes, respectively, of the aliphatic chain of ligands.[28] The feature at *ca.* 2161 cm^{-1} is associated with Si–H bonds in octadecylsilyl-GeNPs. This feature arises as a consequence of excess ligand (see XRD discussion) and as a result of Ge-SiH_2-R surface linkages. For dimethyloctadecylsilyl-GeNPs, no feature associated with Si–H was observed. The H-PDMS-GeNP show a small feature (*ca.* 2127 cm^{-1}) that was expected due to the presence of two Si–H in terminal position of the polymer.

The Raman spectra of alkyl/alkylsilane functionalized GeNPs show strong phonon absorption at *ca.* 299 cm^{-1} that is attributed to a Ge–Ge modes (Fig. 2).[29] Literature reports indicate a Si–Ge optical phonon is expected to appear at *ca.* 400 cm^{-1} in SiGe alloy.[30] However, in the present NPs, one surface layer of Si–Ge bonds does not provide adequate signal for detection. The Raman spectrum of crystalline-Ge (*c*-Ge) is shown for comparison. The shoulder observed from functionalized GeNPs suggests the presence of amorphous content. These observations are consistent with our previous findings related to SiNPs,[31] as well as reports that indicate discrepancies between XRD determined crystallite and TEM particle sizes.[29]

^{1}H-NMR spectroscopy provides insight into the nature of the GeNP surface species. ^{1}H-NMR spectra of octadecyl-GeNPs (Fig. 3a*(i)*) show a set of broad resonances arising from terminal methyl protons (centered at δ = 0.88 ppm), and methylene chain protons (δ = 1.1–1.5 ppm). The integration ratio of the terminal methyl to the methylene chain protons signals

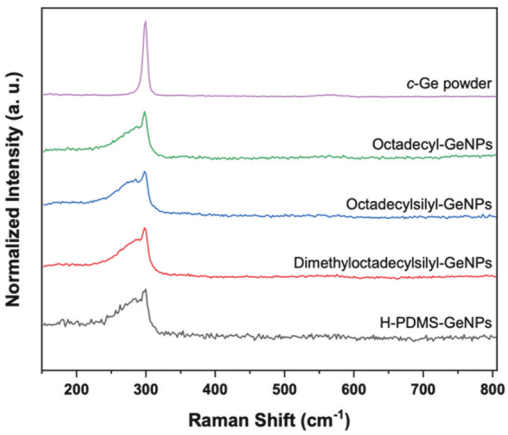

Fig. 2 Raman spectra of *c*-Ge powder, octadecyl-GeNPs, octadecylsilyl-GeNPs, dimethyloctadecylsilyl-GeNPs, and H-PDMS-GeNPs.

(3 : 32.4) is consistent with that of the expected surface octadecyl moieties.

The octadecylsilyl-GeNPs (Fig. 3a*(ii)*) show terminal methyl protons at 0.88 ppm, Si adjacent methylene protons at 0.6 ppm, and methylene protons at 1.1–1.6 ppm (integration ratio 3 : 2.6 : 24.9). It is important to mention that for octadecylsilane, this silane proton shows a resonance at 3.48 ppm (Fig. 3b), which may have shifted to 4.6 ppm upon attachment to GeNP surfaces. In the case of dimethyloctadecylsilyl-GeNPs (Fig. 3a*(iii)*), no silane proton signal was observed. The integration ratio of terminal methyl (at δ = 0.88 ppm) to methylene chain (δ = 1.1–1.6 ppm) to silicon adjacent methylene (δ = 0.56 ppm), and to silicon adjacent methyl (δ = 0.096 ppm) protons was 3 : 31.4 : 1.9 : 5.1, again consistent with the target functionalization. For H-PDMS-GeNPs (Fig. 3a*(iv)*), there was

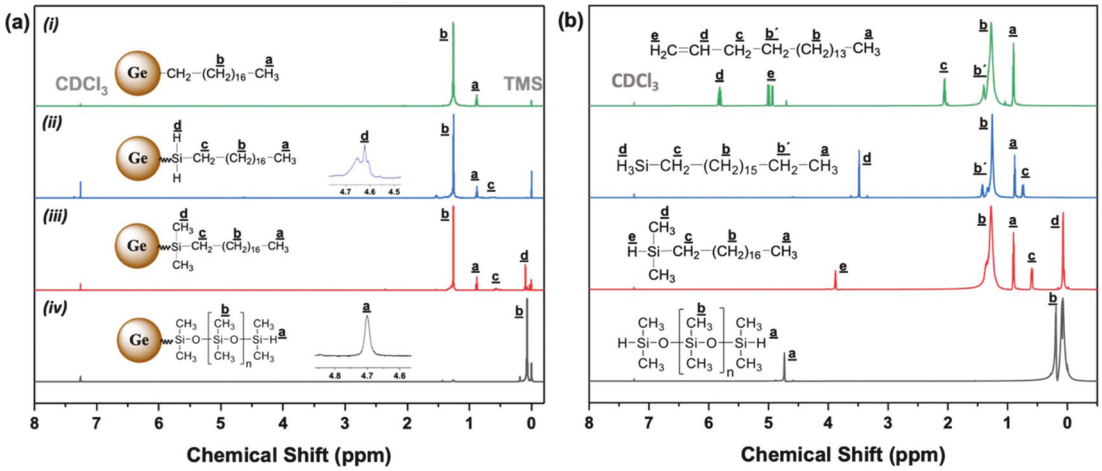

Fig. 3 (a) ^{1}H-NMR of *(i)* octadecyl-GeNPs, *(ii)* octadecylsilyl-GeNPs, *(iii)* dimethyloctadecylsilyl-GeNPs, and *(iv)* H-PDMS-GeNPs in $CDCl_3$ (7.2 ppm) with 0.03% TMS (0.0 ppm) and (b) ^{1}H-NMR of (from top) 1-octadecene, octadecylsilane, dimethyloctadecylsilane, and H-PDMS in $CDCl_3$ (7.2 ppm).

still a resonance arising from the silane proton (δ = 4.70 ppm) due to the presence of two terminal Si–H in the ligand, however, measuring the intensity ratios does not give meaningful information.

Surface coverage was estimated by ^{1}H-NMR *via* using a predefined amount of tetramethylsilane (TMS, 0.03% v/v) as an internal standard and evaluating a ratio of the integrated peak areas of the surface groups provides an estimate of the percent surface coverage. In this context, the average surface coverage of octadecyl-GeNPs, octadecylsilyl-GeNPs, and dimethyloctadecylsilyl-GeNPs obtained from hydrogermylation/dehydrocoupling reaction are 170, 139, and 80.6%, respectively (Tables S1, S2, and S3†). For GeNPs derivatized using thermally induced hydrogermylation, surface oligomerization is known and accounts for >100% surface coverage.[15] Similarly, challenges associated with removal of excess octadecylsilane limits the accuracy of the present surface coverage estimate.

The functionalized GeNP samples, reactants, and intermediate materials were also analyzed using powder X-ray diffraction (XRD). To take account for diffraction contributions arising from Si-wafer sample holders, empty holders were evaluated; all showed broad reflections (Fig. S3a and b†) that were accounted for during sample analysis. In addition to six-polynomial backgrounds, a function describing the sample holder background parameters was added. The diffraction pattern of the $Ge(OH)_2$ precursor shows a broad feature indicative of an amorphous material. The GeNP/GeO_x composite shows Ge (a = 5.64 Å cell parameter, and 7.6 nm crystallite size) and amorphous GeO_2 (a = 5.05 Å and c = 5.37 Å) phases (Fig. S3a†).

The XRD patterns obtained for alkyl/alkylsilane functionalized GeNPs were analyzed with diffraction line-broadening methods to determine the size of crystallites and strain (Fig. 4). After refining the reference, instrument parameters and peak shape values were fixed, and line broadening was assumed to result only from physical features. Size determination from diffraction data were analyzed with integral

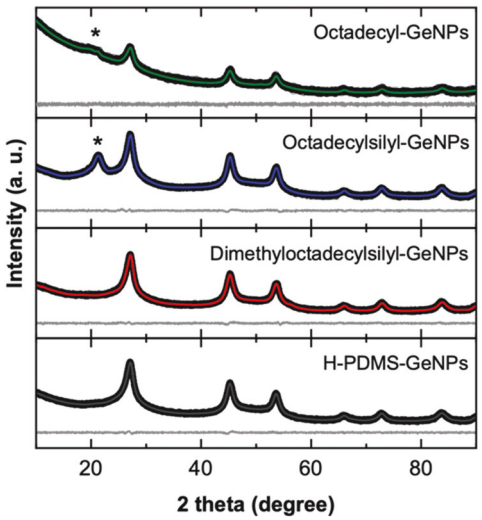

Fig. 4 X-ray diffraction of octadecyl-GeNPs, octadecylsilyl-GeNPs, dimethyloctadecylsilyl-GeNPs, and H-PDMS-GeNPs. * indicates broad reflections arising from organic moiety.

breadth, FWHM, and Lorentzian/Gaussian broadening methods. All the methods assume a normal distribution of spherical crystallites. Strain broadening analysis was performed, and the strain value as defined by Stokes and Wilson was refined.[32,33] Table S4† lists the crystallite sizes/integral breadths of 5.92, 6.52, 7.43, and 7.83 nm for octadecyl-GeNPs, octadecylsilyl-GeNPs, dimethyloctadecylsilyl-GeNPs, and H-PDMS-GeNPs, respectively. The alkyl-GeNPs show smaller strain component than alkylsilane-GeNPs. Again, the dimethyloctadecylsilyl-GeNPs and H-PDMS-GeNPs exhibit larger strain than octadecylsilyl-GeNPs.

The reflections at 27.09°, 45.30°, 53.65°, 65.91°, 72.84°, and 83.65° correspond to cubic germanium (111), (220), (311), (400), (331), and (422) planes, respectively (Fig. 4, PDF# 04-

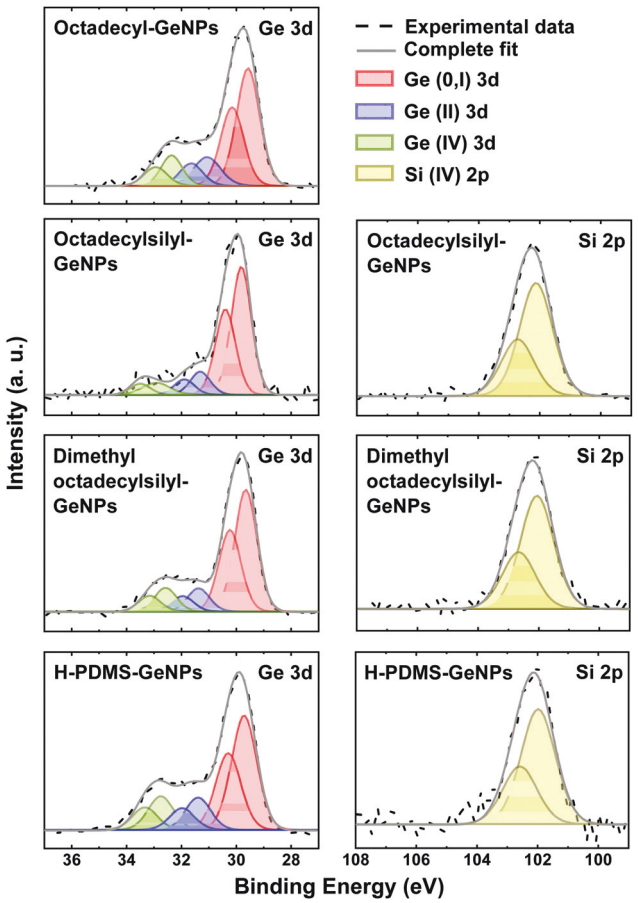

Fig. 5 High-resolution XP spectra of Ge 3d and Si 2p of indicated alkene and alkylsilane functionalized GeNPs.

0545).[34] For octadecyl-GeNPs, two weak reflections at 19.58° and 21.27° were observed. A broad reflection at 21.31° was observed for octadecylsilyl-GeNPs. To identify the origin of this reflection, an XRD of octadecylsilane (melting point 28 °C) was carried out and a reflection was found at the same 2-theta position (Fig. S4†).

The survey X-ray photoelectron (XP) spectra of octadecyl-GeNPs confirms the presence of Ge, C, and O, and all the alkylsilane functionalized GeNPs confirm the presence of Ge, Si, C, and O (Fig. S5 and Table S5†). All XP spectra were calibrated using internal adventitious C 1s at 284.8 eV. The high-resolution XP spectra of the Ge 3d region (Fig. 5) were fit/deconvoluted to components arising from elemental (*i.e.*, Ge(0)) and surface (*i.e.*, Ge(I)) species that appear at *ca.* 29.6 eV. We also note some higher Ge oxidation states arising from some partial oxidation at *ca.* 31.4, and 32.7 eV.[35] Small shifts to higher binding energy (up to 0.3 eV) were observed for alkylsilane functionalized GeNPs compared to alkyl-GeNPs; this is not surprising and is known for cases when using adventitious C 1s as an internal calibration standard.[36–38] The Si 2p region of the high-resolution XP spectrum (Fig. 5) was fit to the $2p_{1/2}$ and $2p_{3/2}$ spin–orbit couple, with a binding energy of *ca.* 102.1 and 102.6 eV, respectively, and can be attributed to alkylsilane attached to GeNPs.[39] The C 1s region also was fit to identify the amount of oxide arising from adventitious carbon (Fig. S6 and Table S6†).

The hydrodynamic radius of all the GeNPs was evaluated using Dynamic Light Scattering (DLS), which shows 23 and 29 nm for octadecyl-GeNPs and octadecylsilyl-GeNPs, respectively (Fig. S7†). In contrast, DLS shows dimensions of 335 and 375 nm for dimethyloctadecylsilyl-GeNPs and H-PDMS-GeNPs

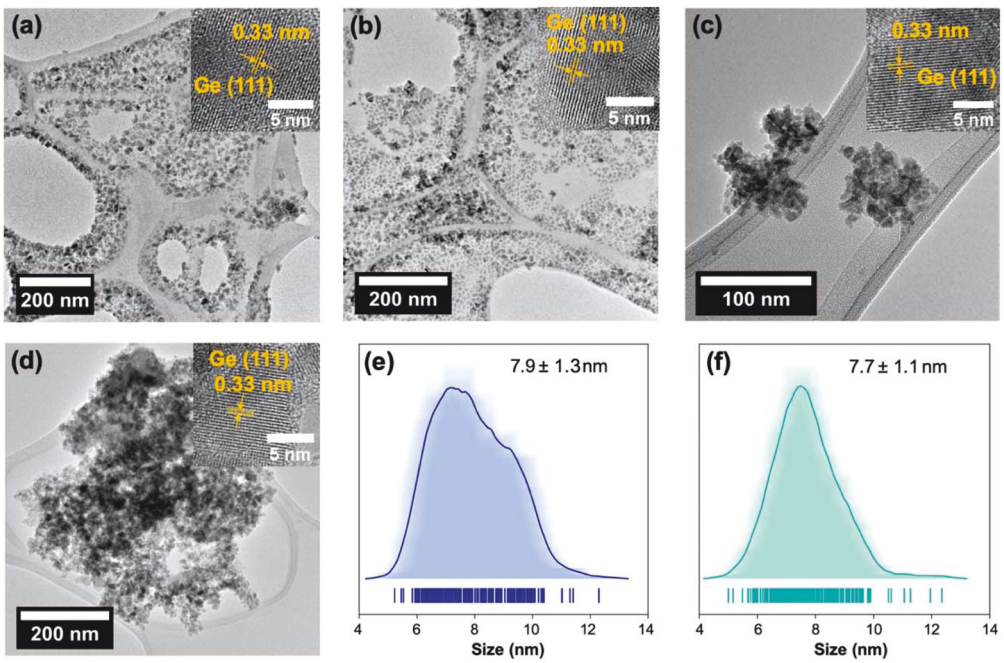

Fig. 6 Brightfield TEM images of (a) octadecyl-GeNPs, (b) octadecylsilyl-GeNPs, (c) dimethyloctadecylsilyl-GeNPs, and (d) H-PDMS-GeNPs (inset: HRTEM) and corresponding Average Shifted Histograms for (e) octadecyl-GeNPs and (f) octadecylsilyl-GeNPs.

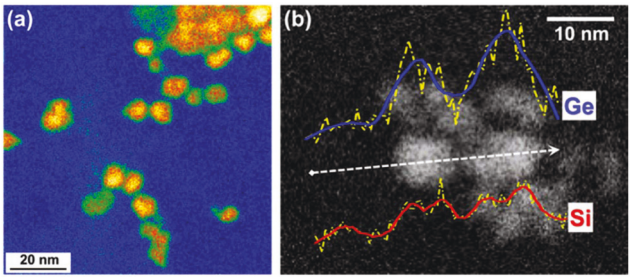

Fig. 7 (a) HAADF image of octadecylsilyl-GeNPs, and (b) EELS line scanning of two single particles showing the composition of the core and shell.

(Fig. S7†), which are consistent with the aggregation noted in brightfield transmission electron microscope (TEM) and suggests crosslinking may happen in H-PDMS-GeNPs.

Direct evaluation of oxide-embedded GeNPs using electron microscopy is impractical, however, inspection of liberated functionalized GeNPs is informative. TEM and high-resolution TEM (HRTEM) give insight into the morphology and local crystallinity of the functionalized NPs of octadecyl-GeNPs, octadecylsilyl-GeNPs, dimethyloctadecylsilyl-GeNPs, and H-PDMS-GeNPs. The GeNPs are randomly shaped and exhibit an average diameter (taken as the longest dimension) of 7.9 ± 1.3 nm for octadecyl-GeNPs (Fig. 6a) and 7.7 ± 1.1 nm for octadecylsilyl-GeNPs (Fig. 6b). The size distributions (Fig. 6e and f) of the particles were measured by average shifted histogram (ASH).[40] It was impractical to measure the size of the dimethyloctadecylsilyl-GeNPs and H-PDMS-GeNPs using TEM because they were aggregated (Fig. 6c and d). HRTEM imaging (Fig. 6a–d, inset) shows crystalline domains with the lattice spacing of 0.33 nm, consistent with the present XRD analysis that correspond to Ge (111) lattice spacing.[15]

To gain more insight into the presence and location of Si at the surface of GeNPs, HAADF imaging and Electron Energy Loss Spectroscopy (EELS) line scans were acquired for octadecylsilyl-GeNPs. HAADF imaging shows a contrast between core and surface materials, consistent with different materials at the particle surface and within the particle core (Fig. 7a). The EELS line scans of two representative single particles indicate the intensities of silicon signals are substantially higher at particle edges, while the composition of the core is dominated by germanium (Fig. 7b).

Conclusions

We have synthesized alkylsilane functionalized GeNPs through DHC reactions that proceed *via* Si–Ge bond formation. FTIR and ^{1}H-NMR show the presence of alkylsilane in the samples. Raman data demonstrates the presence crystalline GeNPs along with some amorphous content. The XRD data shows the presence of crystalline domains in GeNPs. The alkylsilane-GeNPs show higher strain than the alkyl-GeNPs. The XPS shows the presence of silicon, along with germanium. Finally, EELS line scanning confirms the presence of silicon, mostly on the surface of GeNPs. DHC opens the door to a new catalyst free approach to GeNP surface modification and may provide a pathway to realize new functional nanomaterials.

Conflicts of interest

There are no conflicts to declare.

Acknowledgements

The authors acknowledge the continued generous funding from the Natural Sciences and Engineering Research Council of Canada (NSERC) Discovery Grant Program, the NSERC CREATE supported Alberta/Technical University of Munich International Graduate School for Hybrid Functional Materials (ATUMS; CREATE-463990-2015), Future Energy Systems, and the Department of Chemistry at the University of Alberta. We also thank Dr A. Jordan of the University of Alberta for editing assistance.

Notes and references

1 D. D. Vaughn II and R. E. Schaak, *Chem. Soc. Rev.*, 2013, **42**, 2861–2879.
2 Y. J. Cho, H. S. Im, H. S. Kim, Y. Myung, S. H. Back, Y. R. Lim, C. S. Jung, D. M. Jang, J. Park, E. H. Cha, W. Il Cho, F. Shojaei and H. S. Kang, *ACS Nano*, 2013, **7**, 9075–9084.
3 Z. C. Holman, C.-Y. Liu and U. R. Kortshagen, *Nano Lett.*, 2010, **10**, 2661–2666.
4 W. K. Choi, W. K. Chim, C. L. Heng, L. W. Teo, V. Ho, V. Ng, D. A. Antoniadis and E. A. Fitzgerald, *Appl. Phys. Lett.*, 2002, **80**, 2014–2016.
5 T. A. Amollo, G. T. Mola and V. O. Nyamori, *RSC Adv.*, 2018, **8**, 21841–21849.
6 D. A. Grachev, A. V. Ershov, A. V. Belolipetsky, L. V. Krasilnikova, A. N. Yablonskiy, B. A. Andreev and O. B. Gusev, *Phys. Status Solidi*, 2016, **213**, 2867–2872.
7 D.-J. Xue, J.-J. Wang, Y.-Q. Wang, S. Xin, Y.-G. Guo and L.-J. Wan, *Adv. Mater.*, 2011, **23**, 3704–3707.
8 B. F. P. Mc Vey, S. Prabakar, J. J. Gooding and R. D. Tilley, *ChemPlusChem*, 2016, **81**, 60–73.
9 T. Hanrath and B. A. Korgel, *J. Am. Chem. Soc.*, 2004, **126**, 15466–15472.
10 K. Choi and J. M. Buriak, *Langmuir*, 2000, **16**, 7737–7741.
11 J. M. Buriak, *Chem. Rev.*, 2002, **102**, 1271–1308.
12 D. C. Lee, J. M. Pietryga, I. Robel, D. J. Werder, R. D. Schaller and V. I. Klimov, *J. Am. Chem. Soc.*, 2009, **131**, 3436–3437.
13 S. Prabakar, A. Shiohara, S. Hanada, K. Fujioka, K. Yamamoto and R. D. Tilley, *Chem. Mater.*, 2010, **22**, 482–486.
14 H. C. Choi and J. M. Buriak, *Chem. Commun.*, 2000, 1669–1670.

15 M. Javadi, D. Picard, R. Sinelnikov, M. A. Narreto, F. A. Hegmann and J. G. C. Veinot, *Langmuir*, 2017, **33**, 8757–8765.
16 S. Bhattacharjee, I. M. C. M. Rietjens, M. P. Singh, T. M. Atkins, T. K. Purkait, Z. Xu, S. Regli, A. Shukaliak, R. J. Clark, B. S. Mitchell, G. M. Alink, A. T. M. Marcelis, M. J. Fink, J. G. C. Veinot, S. M. Kauzlarich and H. Zuilhof, *Nanoscale*, 2013, **5**, 4870–4883.
17 R. L. Melen, *Chem. Soc. Rev.*, 2016, 775–778.
18 R. Waterman, *Chem. Soc. Rev.*, 2013, **42**, 5629–5641.
19 Y.-H. Li and J. M. Buriak, *Inorg. Chem.*, 2006, **45**, 1096–1102.
20 Z. Yang, M. H. Wahl and J. G. C. Veinot, *Can. J. Chem.*, 2014, **92**, 951–957.
21 D. Kim, J. Joo, Y. Pan, A. Boarino, Y. W. Jun, K. H. Ahn, B. Arkles and M. J. Sailor, *Angew. Chem., Int. Ed.*, 2016, **55**, 6423–6427.
22 C. Aitken, J. F. Harrod, A. Malek and E. Samuel, *J. Organomet. Chem.*, 1988, **349**, 285–291.
23 E. L. de Oliveira, E. L. Albuquerque, J. S. de Sousa, G. A. Farias and F. M. Peeters, *J. Phys. Chem. C*, 2012, **116**, 4399–4407.
24 J. T. Held, K. I. Hunter, N. Dahod, B. Greenberg, D. Reifsnyder Hickey, W. A. Tisdale, U. Kortshagen and K. A. Mkhoyan, *ACS Appl. Nano Mater.*, 2018, **1**, 989–996.
25 K. I. Hunter, J. T. Held, K. A. Mkhoyan and U. R. Kortshagen, *ACS Appl. Mater. Interfaces*, 2017, **9**, 8263–8270.
26 C. Mehringer, C. Kloner, B. Butz, B. Winter, E. Spiecker and W. Peukert, *Nanoscale*, 2015, **7**, 5186–5196.
27 M. Eshed, K. Keinan-Adamsky, G. Goobes and A. Gedanken, *J. Phys. Chem. C*, 2013, **117**, 11086–11094.
28 Z. Yang, C. M. Gonzalez, T. K. Purkait, M. Iqbal, A. Meldrum and J. G. C. Veinot, *Langmuir*, 2015, **31**, 10540–10548.
29 A. Bernard, K. Zhang, D. Larson, K. Tabatabaei and S. M. Kauzlarich, *Inorg. Chem.*, 2018, **57**, 5299–5306.
30 Z. Sui, H. H. Burke and I. P. Herman, *Phys. Rev. B: Condens. Matter Mater. Phys.*, 1993, **48**, 2162–2168.
31 A. N. Thiessen, M. Ha, R. W. Hooper, H. Yu, A. O. Oliynyk, J. G. C. Veinot and V. K. Michaelis, *Chem. Mater.*, 2019, **31**, 678–688.
32 D. Balzar, N. Audebrand, M. R. Daymond, A. Fitch, A. Hewat, J. I. Langford, A. Le Bail, D. Louër, O. Masson, C. N. McCowan, N. C. Popa, P. W. Stephens and B. H. Toby, *J. Appl. Crystallogr.*, 2004, **37**, 911–924.
33 A. R. Stokes and A. J. C. Wilson, *Proc. Phys. Soc.*, 1944, **56**, 174–181.
34 M. Javadi, V. K. Michaelis and J. G. C. Veinot, *J. Phys. Chem. C*, 2018, **122**, 17518–17525.
35 Y. Wang, U. Ramesh, C. K. A. Nyamekye, B. J. Ryan, R. D. Nelson, A. M. Alebri, U. H. Hamdeh, A. Hadi, E. A. Smith and M. G. Panthani, *Chem. Commun.*, 2019, **55**, 6102–6105.
36 P. Swift, *Surf. Interface Anal.*, 1982, **4**, 47–51.
37 T. L. Barr and S. Seal, *J. Vac. Sci. Technol., A*, 1995, **13**, 1239–1246.
38 D. J. Miller, M. C. Biesinger and N. S. McIntyre, *Surf. Interface Anal.*, 2002, **33**, 299–305.
39 N. Shirahata, W.-S. Seo, T. Kinoshita, T. Yonezawa, A. Hozumi, Y. Yokogawa, T. Kameyama, Y. Masuda and K. Koumoto, *Langmuir*, 2004, **20**, 8942–8946.
40 S. L. Anderson, E. J. Luber, B. C. Olsen and J. M. Buriak, *Chem. Mater.*, 2016, **28**, 5973–5975.